Chaotic Excitation and Tidal Damping in the GJ 876 System

Abhijit Puranam and Konstantin Batygin
Division of Geological and Planetary Sciences, California Institute of Technology, Pasadena, CA 91125, USA; kbatygin@gps.caltech.edu

Abstract

The M-dwarf GJ 876 is the closest known star to harbor a multi-planetary system. With three outer planets locked in a chaotic Laplace-type resonance and an appreciably eccentric short-period super-Earth, this system represents a unique exposition of extrasolar planetary dynamics. A key question that concerns the long-term evolution of this system, and the fate of close-in planets in general, is how the significant eccentricity of the inner-most planet is maintained against tidal circularization on timescales comparable to the age of the universe. Here, we employ stochastic secular perturbation theory and N-body simulations to show that the orbit of the inner-most planet is shaped by a delicate balance between extrinsic chaotic forcing and tidal dissipation. As such, the planet's orbital eccentricity represents an indirect measure of its tidal quality factor. Based on the system's present-day architecture, we estimate that the extrasolar super-Earth GJ 876 d has a tidal $Q \sim 10^4$–10^5, a value characteristic of solar system gas giants.

Key words: chaos – planetary systems – planets and satellites: dynamical evolution and stability

1. Introduction

The study of main-sequence exoplanetary systems began with the detection of the first hot Jupiter, 51 Peg b, in 1995 (Mayor & Queloz 1995). At the time, the detection of these massive, close-in planets defied the conventional theory of planet formation (Pollack et al. 1996). The development of planet migration theory (Goldreich & Tremaine 1980), however, helped explain the existence of hot Jupiters and furthered the understanding of the physical processes that operate concurrently with planet formation[1] (Lin et al. 1996).

Among the earliest hot Jupiters to be detected was GJ 876b, a 2.2 M_J planet orbiting an M-dwarf at 0.2 au with a period of $P = 60$ days (Marcy et al. 1998). Subsequently, GJ 876 c, a 0.7 M_J planet orbiting at 0.13 au, was discovered in a 2:1 orbital resonance with 876 b (Marcy et al. 2001). This discovery made the GJ 876 planetary system not only an ideal testing ground for theories of planetary formation and migration, but also an unusual example of a close-in giant planet system (Fischer & Valenti 2005).

Further characterization of the system revealed GJ 876 d, a super-Earth with a semimajor axis of 0.02 au, and an exterior Uranus-mass planet GJ 876 e (Rivera et al. 2005, 2010). GJ 876 e orbits at 0.35 au with a period of $P = 120$ days, making the c-b-e triplet a Laplace-type resonance. Against the backdrop of the planetary population discovered by the *Kepler* mission, it is evident that rather than a typical member of the galactic planetary census, the GJ 876 system stands out as a remarkable anomaly worthy of closer examination.

The GJ 876 system is unique because (1) Jupiter-class planets are generally rare around M-dwarf stars (Valenti & Fischer 2005) and (2) the c-b-e Laplace resonance exhibits rapid dynamical chaos, unlike the well-ordered Laplace resonance of the Galilean moons of Jupiter (Batygin et al. 2015a). Additionally, the short-period super-Earth GJ 876 d exhibits an intriguingly moderate eccentricity of $e_d = 0.05$–0.15 (Correia et al. 2010; Nelson et al. 2016;

Millholland et al. 2018; Trifonov et al. 2018). As we show below, any finite eccentricity is at odds with the standard model of tidal dissipation. Accordingly, this study focuses on the origins of this peculiar orbital architecture. Specifically, here we show that chaotic excitations arising from the Laplace-like resonance of the c-b-e chain are instrumental toward explaining the eccentricity of 876 d, and this behavior yields constraints on the planet's tidal quality factor.

The paper is structured as follows. In Section 2, we discuss our numerical experiments and characterize the dynamical behavior of the system. In Section 3, we employ stochastic perturbation theory to model and support the results of our numerical experiments. We conclude and discuss our results in Section 4.

2. Numerical Experiments

The physical parameters of the GJ 876 system have been refined continuously since its discovery. For the purposes of this work, we have adopted the recent fit of orbital parameters from Nelson et al. (2016). This fit is based on Doppler velocity measurements and results in an orbital configuration that exhibits long-term stability.

Our numerical simulations utilized the *Symba* symplectic gravitational dynamics software package, based on the work of Wisdom & Holman (1991) and Duncan et al. (1998). In order to properly model short-range planet–star interactions, the code has been modified to account for general relativistic effects (Nobili & Roxburgh 1986) and to include tidal effects using the constant time-lag formalism outlined by Mignard (1980); Hut (1981). In particular, dissipative effects were self-consistently taken into account by introducing velocity-dependent forces into the equations of motion, while ensuring that total (spin plus orbital) angular momentum remains conserved (Mardling & Lin 2002). For all integrations, we adopted a timestep of 0.1 days—approximately 1/20 of the inner-most planet's orbital period.

---

[1] The extent to which hot Jupiters migrate within their natal disks remains an open question, as both in situ and ex situ formation models have been suggested (Batygin et al. 2016).

Table 1
Adopted Orbital Fit of the GJ 876 System.

	M ($M_\odot$)	a (au)	e	$\mathcal{M}$ (deg)	ϖ (deg)
$\star$	0.37				
d	2.25×10^{-5}	0.02	0.12	301.87	219.10
c	7.99×10^{-4}	0.13	0.25	139.32	115.96
b	2.54×10^{-3}	0.21	0.03	74.62	110.86
e	4.98×10^{-5}	0.35	0.03	184.11	129.56

2.1. Tidal Evolution

In the absence of external gravitational perturbations, the tidal evolution of eccentricity occurs on a characteristic timescale (Yoder & Peale 1981):

$$\left(\frac{1}{e}\frac{de}{dt}\right)^{-1} = \left(\frac{1}{n}\right)\left(\frac{2}{21}\right)\left(\frac{m}{M_\star}\right)\left(\frac{a}{R}\right)^5\left(\frac{Q}{k_2}\right) = \tau_e, \qquad (1)$$

where n is the mean motion, a is the semimajor axis, R is the radius of the orbiting body, Q is the tidal dissipation quality factor, and k_2 is the Love number. We note that in addition to eccentricity damping, tidal dissipation also facilitates semimajor axis decay. However, this process unfolds on a much longer characteristic timescale: $\tau_a = \tau_e/2\, e^2 \sim 30\, \tau_e$ and can be neglected for the moment (our numerical experiments will treat tidal dissipation self-consistently).

Expression (1) indicates that in the presence of only tidal forcing, a planet's eccentricity will exhibit nearly exponential decay. Calculating the true circularization timescale of an exoplanet directly using this expression, however, is abortive because first-principles based estimates of the tidal quality factor remain elusive, with lack of constraints on the planetary composition further aggravating the uncertainty. Instead, the oft-cited estimates tidal Q are based on observations of bodies within our own solar system (Goldreich & Soter 1966), with no faithful point of comparison for the tidal quality factor of 876 d, a super-Earth.

To motivate further calculations, let us first consider a scenario where the only relevant forcing on eccentricity comes from tidal dissipation. The dynamics would then be described by Equation (1), and the currently observed high eccentricity would be due to a tidal dissipation timescale on the order of the lifetime of the system, about 10 Gyr. Using the mass and orbital parameters from Table (1), we may draw upon the exoplanet mass–radius relationship obtained by Weiss et al. (2013) to estimate a planetary radius of $R \sim 3\, R_\oplus$. Then, using a Love number of $k_2 \sim 0.4$ (Dermott et al. 1988; Banfield & Murray 1992), we obtain a tidal quality factor on the order of $Q \gtrsim 3 \times 10^6$. This is a value considerably larger than that of solar system gas giants, so either 876 d is more than an order of magnitude less dissipative than these planets, or other factors must be important to the evolution of 876 d's eccentricity. Let us consider this alternative.

Our first numerical experiment aims to examine the evolution of GJ 876 d's eccentricity in consideration of tidal forcing from its host star and the periodic gravitational perturbations of the giant planets in the system. We do this by considering the system in a nonchaotic regime by removing 876 e from our calculations. This renders the evolution of planets b and c strictly periodic, because the stochastic evolution of 876 e defines the chaotic nature of the system (Batygin et al. 2015a). At the same time, planet e's low mass
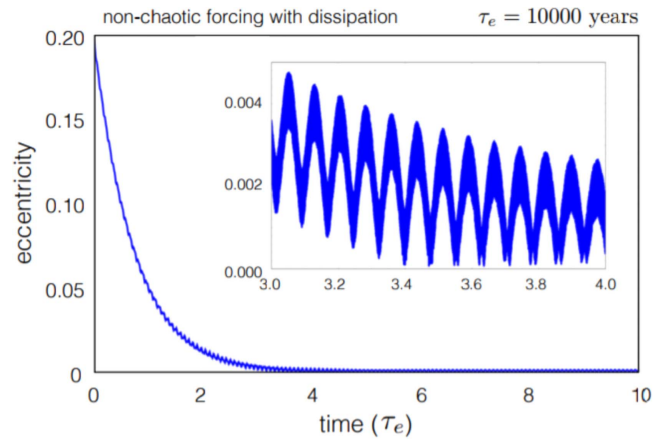

Figure 1. Evolution of GJ 876 d's eccentricity subject to tidal dissipation as well as periodic gravitational forcing from planets b and c. The simulation was performed with initial eccentricity of 0.2 and a tidal timescale of $\tau_e = 10{,}000$ years.

and significant distance from 876 d result in negligible direct influence on the evolution of 876 d's orbit. Thus, the results of these simulations elucidate the behavior of 876 d's eccentricity in the absence of chaotic effects.

In our numerical experiments, we used shorter circularization times than those implied by conventional theory, so that many dynamical timescales can be simulated with less computation time. We note that this adjustment is valid as long as the timescales associated with angular momentum exchange among the planets remain much shorter than the circularization timescales we have adopted.

The results of a representative simulation are shown in Figure 1. Clearly, this calculation yields no explanation for the high eccentricity of planet d. That is, in presence of tidal forcing, no significant excitations in eccentricity exist. Instead, the behavior of 876 d's eccentricity is governed by the exponential decay from tides with small periodic perturbations from the outer planets. Thus, strictly periodic gravitational perturbations from the outer giant planets alone cannot explain the high eccentricity that is observed.

2.2. Chaotic Dynamics

We now consider the full system and its chaotic behavior. Unlike the simulation shown in Figure 1, here we model the full planetary system without considering tidal forces. Our results, shown in Figure 2, demonstrate that chaotic forcing alone is enough to drive eccentricity of 876 d to the observed value on a timescale of a few million years, much less than the lifetime of the system.

With this insight into the importance of chaotic forcing, we perform our tidal dissipation numerical experiment again, this time accounting for the presence of 876 e. The behavior of planet d's eccentricity in this case is shown in Figure 3. While the dominant exponential decay of the eccentricity is similar, the periodic perturbations that manifested in the first experiment are replaced by chaotic excitations in the second experiment. Correspondingly, at sufficiently low eccentricities, these chaotic excitations dominate the behavior over the exponential decay of the tidal forcing.

To quantify this relationship between the tidal and chaotic forcing, we ran a series of simulations sequentially increasing τ_e. A range of 20 different tidal circularization timescales were
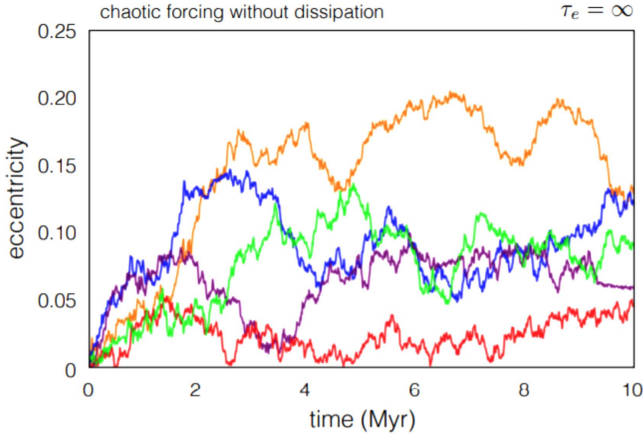
Figure 2. Chaotic evolution of GJ 876 d's eccentricity using randomly generated initial mean anomalies. Note that in absence of tidal effects, the chaotic eccentricity excitation timescale is orders of magnitude shorter than the multi-Gyr age of the system.
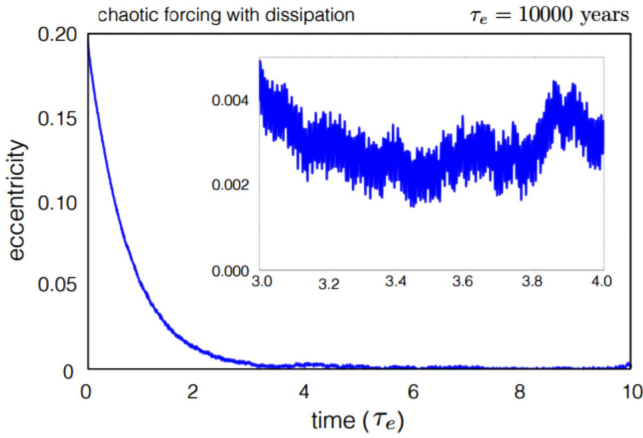

Figure 3. Chaotic Evolution of GJ 876 d's eccentricity in presence of tidal dissipation. The simulation was performed at an initial eccentricity of 0.2 with a tidal timescale of 10000 years.

taken, and for each one, the simulation was performed over 10 circularization timescales. The chaotic nature of the system is acutely sensitive to initial conditions, making it difficult to extract precise information from the system at different circularization timescales—that is, each simulation is only representative of the true evolution of the system in a statistical sense. To account for these effects, 10 simulations were performed at every timescale, with a randomly generated initial mean anomaly for 876 d's orbit.[2] The results are shown in Figure 4, where rms eccentricity of planet d (measured over the last seven circularization timescales) is depicted as a function of τ_e. Clearly, as circularization time is increased, the mean eccentricity attained by planet d also grows. Quantifying this relationship is the focus of the next section.

3. Analytic Theory

3.1. Stochastic Secular Perturbation Theory

Numerical experiments presented in the preceding section suggest that the average eccentricity acquired by planet d after

---

[2] Given the purely secular nature of gravitational coupling between planet d and the remainder of the system, changing its mean anomaly has no qualitative impact on the ensuing dynamical evolution.
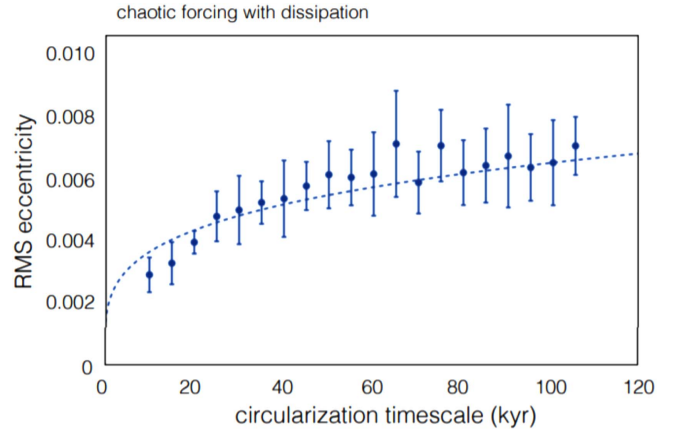

Figure 4. Rms eccentricity of planet d, as a function of tidal decay timescale. The depicted points and error-bars, respectively, denote the mean and the standard deviation of the rms eccentricity sampled across 10 simulations at each circularization timescale. Our suite of numerical experiments reveals a monotonically increasing relationship between that the root mean square eccentricity of 876 d and the tidal damping timescale.

a period of chaotic equilibration is a monotonically increasing function of τ_e. To understand this relationship from analytic grounds, in this section we construct a simplified, perturbative model for the inner-most planet's motion. Given the large separation between the semimajor axes of planets d and c (as well as b) and the lack of a low-order commensurability between the orbital periods, it is sensible to assume that the interactions between these objects are secular in nature. Accordingly, in order to obtain a handle on the dynamical evolution of planet d, we employ Lagrange–Laplace perturbation theory (Murray & Dermott 1999).

To second order in the orbital eccentricities, the secular Hamiltonian that governs GJ 876 d's evolution reads:

$$\mathcal{H} = \frac{-1}{\sqrt{\mathcal{G}Ma}} \frac{\mathcal{G}m'}{4} \left(\frac{a}{a'}\right)^2 [b_{3/2}^{(1)}\,\Gamma - b_{3/2}^{(2)}e'\,\sqrt{2\,\Gamma}\,\cos(\xi\,t - \gamma)] \qquad (2)$$

where b's are Laplace coefficients, $\Gamma = 1 - \sqrt{1-e^2} \simeq e^2/2$ and $\gamma = -\varpi$ are scaled Poincaré action-angle variables corresponding to planet d, while the primed quantities correspond to the perturbing body (i.e., planet c or b). For definitiveness, we assume that e' is nearly constant and the rate of the perturbing planet's pericenter regression, ξ, is time-independent. We note that both of these assumptions are justified by numerical simulations and simultaneously apply to planets b and c, as these objects have co-linear apsidal lines (Correia et al. 2010; Batygin et al. 2015a).

To leading order in the semimajor axis ratio, Hamilton's equation for planet d's longitude of perihelion is:

$$\frac{d\gamma}{dt} = \frac{\partial \mathcal{H}}{\partial \Gamma} \simeq -\frac{3}{4}n\left(\frac{m'}{M}\right)\left(\frac{a}{a'}\right)^3 + \mathcal{O}\left(\frac{a}{a'}\right)^4, \qquad (3)$$

where n is the mean motion of planet d, and we have expanded the Laplace coefficient as a hypergeometric series to leading order. Using Equation (3), it is trivial to check that $|d\gamma/dt| \ll \xi$. This disparity in precession frequencies explains why no coherent angular momentum exchange can be seen in Figure 1. That is, resonantly induced rapid regression of planet

b and c's pericenter essentially renders the secular harmonic of Hamiltonian (2) a short-periodic effect that can be averaged over.

Accounting for the tidal decay of the orbital eccentricity (e.g., Hut 1981), the equation of motion for planet d's angular momentum deficit reads:

$$\frac{d\Gamma}{dt} = -\frac{\partial H}{\partial \gamma} + \frac{\partial \Gamma}{\partial e}\left(\frac{de}{dt}\right)_{\text{tide}}$$

$$\simeq \frac{15}{8\sqrt{2}} n \left(\frac{a}{a'}\right)^4 e' \sqrt{\Gamma} \sin(\xi\, t) - 2\frac{\Gamma}{\tau_e}, \qquad (4)$$

where we have neglected the slow evolution of γ and adopted ξ as the harmonic circulation frequency. Averaged over time-scales much longer than $2\pi/\xi$, chaotic variation in $e' \sin(\xi\, t)$, that arises from perturbations due to planet e, can be crudely modeled as a drift-free Weiner process, $\mathcal{W}$ (Batygin et al. 2015b). Under this prescription, Equation (4) reduces to a readily integrable stochastic differential equation:

$$d\langle \Gamma \rangle = 2\sqrt{\mathcal{D}\langle \Gamma \rangle}\, d\mathcal{W} - 2\frac{\langle \Gamma \rangle}{\tau_e} dt, \qquad (5)$$

where $\langle \Gamma \rangle$ denotes the time-averaged angular momentum deficit, and $\mathcal{D}$ is an effective diffusion coefficient that encompasses the chaotic nature of the perturbing orbits.

The standard deviation of the distribution function arising from Equation (5) is given by

$$\sigma_{\langle \Gamma \rangle} = \sqrt{2\,\langle \Gamma_0 \rangle\, \mathcal{D}\,\tau_e (\exp(-2t/\tau_e) - \exp(-4t/\tau_e))}, \qquad (6)$$

where $\langle \Gamma_0 \rangle \neq 0$ is an (arbitrary) initial condition. The function (7) has a global maximum at $t = \log(2)\tau_e/2$, and asymptotically approaches zero as $t \to \infty$. This long-term behavior is unphysical and stems from the fact that $\langle \Gamma \rangle = 0$ is an absorbing boundary in Equation (5), while in reality it is reflective (i.e., a path that encounters $\langle \Gamma \rangle = 0$ within the framework of Equation (5) will remain at $\langle \Gamma \rangle = 0$ for all subsequent time, whereas real circular orbits can become eccentric[3]). Here, we circumvent this artificial limitation simply by evaluating $\sigma_{\langle \Gamma \rangle}$ at its global maximum. Then, the standard deviation of the stochastic process (5) becomes

$$(\sigma_{\langle \Gamma \rangle})_{\text{max}} = \sqrt{\langle \Gamma_0 \rangle\, \mathcal{D}\,\tau_e/2}. \qquad (7)$$

The key result of the above analysis is that the average eccentricity of planet d scales as the quarter-root of the circularization timescale:

$$\langle e \rangle \underset{\sim}{\propto} \tau_e^{1/4}. \qquad (8)$$

Note that this scaling was derived exclusively under the assumption of secular perturbations arising from a chaotic companion and should therefore be applicable even if planet d experiences a limited degree of inward tidal migration over the lifetime of the system. The relationship (8) is shown as a blue dashed line in Figure 4, and clearly provides an adequate match to our suite of numerical simulations, allowing us to extrapolate the existing results to more realistic values of τ_e.

---

[3]   This unphysical behavior results from decoupling Hamilton's equations from one another, and only manifests as a practical issue at very low eccentricities, where $d\gamma/dt$ can become arbitrarily large.
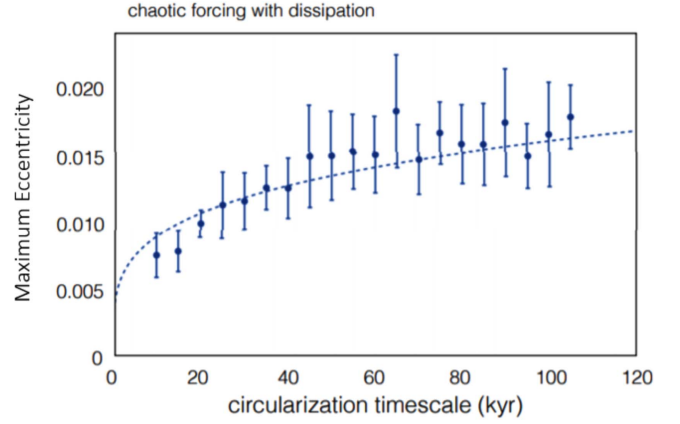

Figure 5. The maximum eccentricity achieved as a function of tidal timescale for our numerical experiment. As in Figure 4, the depicted points and error-bars, respectively, denote the mean and the standard deviation of the maximal eccentricity sampled across 10 simulations at each circularization timescale. The results follow the analytically expected quarter-root relationship indicated by the dashed line.

3.2. A Lower Bound on Tidal Q

The preceding theory can be combined with the results of the numerical experiment described in Section 2.2 to estimate the lower bound of GJ 876 d's tidal quality factor. Specifically, within the context of our N-body simulations, the maximum value of the eccentricity attained by planet d over the modeled $10\tau_e$ integration period is well fit by a quarter-root function:

$$\langle e \rangle = 9.1 \times 10^{-4} \left(\frac{\tau_e}{\text{years}}\right)^{1/4}. \qquad (9)$$

This relationship, shown in Figure 5, can readily be extrapolated to the observed eccentricity to determine an approximate lower bound on the tidal circularization timescale of GJ 876 d. Using the parameters described in Table (1), we estimate that the maximum circularization timescale is of order $\tau_e \sim 3 \times 10^8$ years. Applying this value to Equation (1) and assuming a planetary radius of $3\,R_\oplus$ (Weiss et al. 2013) and a Love number of $k_2 = 0.4$ as before (Dermott et al. 1988; Banfield & Murray 1992), we obtain a lower bound on the tidal quality factor of order $Q \sim 10^5$.

4. Discussion

In this paper, we have examined the origins of the suspiciously finite eccentricity of GJ 876 d and identified the dynamical mechanism that allows for a non-zero eccentricity to be maintained against tidal dissipation. This mechanism relies on the rapid chaotic diffusion of the perturbing planets, and thus requires a short Lyapunov time to operate. This means that the described mechanism is specific to the orbital architecture of the GJ 876 system, with no dynamical equivalent existing within the solar system.

The tidal Q we have obtained is in essence a lower bound and represents the first purely dynamical derivation of the specific dissipation function of a super-Earth. This analysis compliments the recent findings of Morley et al. (2017), who have derived a $Q \sim 10^5$ for GJ436b, a Neptune-mass extrasolar planet. Within an order of magnitude, these values also agree with the values of Q derived for solar system ice-giants (Murray & Dermott 1999).

GJ 876 d does not transit its host star, so we were forced to make an assumption about the planetary radius in order to estimate tidal Q. In the relevant mass range, the extrasolar radius–mass data used by Weiss et al. (2013) indicates that the true radius of GJ 876 d could feasibly lie in the range of 2–$3.5 R_\oplus$, although detailed models of Valencia et al. (2007) indicate that the radius could in principle lie below $2 R_\oplus$. In particular, this would lead our lower-bound estimate of tidal quality to range from order 10^4 to order 10^6. Unfortunately, without direct measurements of the planetary radius and interior density distribution, it is impossible to derive tighter empirical constraints on this value, leaving our fiducial $Q \sim 10^5$ estimate of the quality factor highly uncertain.

Additional ambiguity in our calculations arises from the fact that the eccentricity of planet d itself is relatively poorly constrained by the radial velocity data. To this end, the recent analyses of Trifonov et al. (2018) and Millholland et al. (2018) favor a somewhat lower eccentricity than that derived by Nelson et al. (2016) i.e., $e_d \approx 0.06$–0.08. This revision implies a considerably shorter circularization timescale of $\tau_e \sim 20$ Myr, which in turn translates to a lower estimate of the tidal quality factor ($Q \sim 10^4$ for our adopted parameters). We further note that we have assumed coplanarity within the system, and while a null mutual inclination between planets is expected based upon the inferred early dynamical evolution of the GJ 876 b–c resonance (Lee & Peale 2002), a significant orbital misalignment would further complicate the interpretation of GJ 876 d's non-zero eccentricity.

We conclude by pointing out that although the orbital architecture of the GJ 876 system itself is a relatively rare outcome of planet formation, it is almost certainly non-unique. That is, both multi-planetary resonant chains (e.g., Kepler-60 and Kepler-223) as well as rapidly chaotic systems, such as Kepler-36 (Deck et al. 2012) are present within the Galactic planetary census. This means that the dynamical calculation of tidal Q presented herein is generally not limited to the GJ 876 system and will be applicable to other extrasolar systems as they continue to be discovered. In particular, an application of the derived methodology to transiting multi-planet systems would provide a viable avenue for further constraining the efficiency of tidal dissipation of extrasolar planets.

References

Banfield, D., & Murray, N. 1992, Icar, 99, 390
Batygin, K., Bodenheimer, P. H., & Laughlin, G. P. 2016, ApJ, 829, 114
Batygin, K., Deck, K. M., & Holman, M. J. 2015a, AJ, 149, 167
Batygin, K., Morbidelli, A., & Holman, M. J. 2015b, ApJ, 799, 120
Correia, A. C. M., Couetdic, J., Laskar, J., et al. 2010, A&A, 511, A21
Deck, K. M., Holman, M. J., Agol, E., et al. 2012, ApJL, 755, L21
Dermott, S. F., Malhotra, R., & Murray, C. D. 1988, Icar, 76, 295
Duncan, M. J., Levison, H. F., & Lee, M. H. 1998, AJ, 116, 2067
Fischer, D. A., & Valenti, J. 2005, ApJ, 622, 1102
Goldreich, P., & Soter, S. 1966, Icar, 5, 375
Goldreich, P., & Tremaine, S. 1980, ApJ, 241, 425
Hut, P. 1981, A&A, 99, 126
Lee, M. H., & Peale, S. J. 2002, ApJ, 567, 596
Lin, D. N. C., Bodenheimer, P., & Richardson, D. C. 1996, Natur, 380, 606
Marcy, G. W., Butler, R. P., Fischer, D., et al. 2001, ApJ, 556, 296
Marcy, G. W., Butler, R. P., Vogt, S. S., Fischer, D., & Lissauer, J. J. 1998, ApJL, 505, L147
Mardling, R. A., & Lin, D. N. C. 2002, ApJ, 573, 829
Mayor, M., & Queloz, D. 1995, Natur, 378, 355
Mignard, F. 1980, M&P, 23, 185
Millholland, S., Laughlin, G., Teske, J., et al. 2018, arXiv:1801.07831
Morley, C. V., Knutson, H., Line, M., et al. 2017, AJ, 153, 86
Murray, C., & Dermott, S. 1999, Solar System Dynamics (Cambridge: Cambridge Univ. Press)
Nelson, B. E., Robertson, P. M., Payne, M. J., et al. 2016, MNRAS, 455, 2484
Nobili, A., & Roxburgh, I. W. 1986, in IAU Symp. 114, Relativity in Celestial Mechanics and Astrometry: High Precision Dynamical Theories and Observational Verifications, ed. A. Kovalevsky & V. A. Brumberg (Dordrecht: Reidel), 105
Pollack, J. B., Hubickyj, O., Bodenheimer, P., et al. 1996, Icar, 124, 62
Rivera, E. J., Laughlin, G., Butler, R. P., et al. 2010, ApJ, 719, 890
Rivera, E. J., Lissauer, J. J., Butler, R. P., et al. 2005, ApJ, 634, 625
Trifonov, T. & 168 colleagues 2018, A&A, 609, A117
Valencia, D., Sasselov, D. D., & O'Connell, R. J. 2007, ApJ, 656, 545
Valenti, J. A., & Fischer, D. A. 2005, ApJS, 159, 141
Weiss, L. M., Marcy, G. W., Rowe, J. F., et al. 2013, ApJ, 768, 14
Wisdom, J., & Holman, M. 1991, AJ, 102, 1528
Yoder, C. F., & Peale, S. J. 1981, Icar, 47, 1